Frequency Spectrum of the Human Head - Neck System

A. Charalambopoulos, G. Dassios, D.I. Fotiadis
and C.V. Massalas

8-96

Preprint no. 8-96/1996

Department of Computer Science
University of Ioannina
45 110 Ioannina, Greece

FREQUENCY SPECTRUM OF THE HUMAN HEAD - NECK SYSTEM

A. CHARALAMBOPOULOS
Institute of Chemical Engineering and High Temperature Chemical Processes, GR 265 00 Patras, Greece

G. DASSIOS
Dept. of Chemical Engineering, University of Patras and Institute of Chemical Engineering and High Temperature Chemical Processes, GR 265 00 Patras, Greece

D.I. FOTIADIS
Dept. of Computer Science, University of Ioannina, GR 451 10 Ioannina ,Greece

and

C.V. MASSALAS*
Dept. of Mathematics, University of Ioannina, GR 451 10 Ioannina, Greece

Abstract

A three-dimensional model of human skull - brain system has been extended to include neck support. The model is based on the assumption of having a hollow sphere (skull), the behaviour of which is described by the elasticity solution, filled with an inviscid, irrotational fluid (cerebrospinal fluid), whose motion is described by the wave equation. The neck is approximated by an elastic support which reacts in three-dimensions. The problem is solved numerically for the eigenfrequency spectra and the results obtained are compared with the existing experimental ones showing good agreement. The role of the various system parameters is also investigated.

* Author to whom correspondence should be addressed

1. INTRODUCTION

The knowledge of how and why the natural frequencies of the human head change is very important and could aid in the development of a new medical instrument for the early diagnosis of the brain diseases (Guarino, 1982). Numerous mathematical and numerical techniques have been developed to study the dynamic characteristics as well as various response characteristics of the human head. The complexity of the cranial system presents an extremely difficult task to one wishing to perform detailed simulation of the physical processes of the human head by mathematical modelling. For this reason geometrical approximations are typically used for analytical investigations (Huston and Seras, 1981, Kabo and Goldsmith, 1983, Merill et al., 1984, Misra and Chakravarty, 1985, Charalambopoulos et al., 1996a,b).

In most of the studies related to the response of the human head made so far by previous investigators through the consideration of mathematical or experimental models, the head was considered to be free-floating system. But in reality, the motion of the head is controlled by the neck as well as its muscles and ligaments. The role of the neck on the response of the cranial system has been first discussed by Landkof et al. (1976) and followed by Reber and Goldsmith (1979).

Landkof et al. (1976) studied a non-destructive axisymmetric impact problem by using mathematical and experimental models. In the models considered by Landkof et al. (1976) the shell representing the skull was assumed to be elastic, isotropic, homogeneous and perfectly spherical in shape; the fluid contained in the shell, representing the brain material was considered to be inviscid and compressible with its motion irrotational. The effect of the neck was included through the consideration of a linear viscoelastic cantilever beam rigidly connected to the shell. Lubock and Goldsmith (1980) studied experimentally the response of two different fluid - filled head-neck models to impact and provided information concerning the validity of the widely prevalent cavitation hypothesis of brain damage. The potential deleterious effects of the helmet mass and inertia through increased head rotations during high acceleration periods were studied by Huston and Sears (1981). Kabo and Goldsmith (1983) constructed a reproducible, synthetic replica of the human head and neck system utilising a water - filled cadaver skull mounted on fibreglass - reinforced and supported by passive silicone rubber muscle and ligament elements in order to study the response of a human head-neck model to transient saggital plane loading. Merrill et al. (1984) presented a three - dimensional model of the head - neck system and developed a numerical method that permits the evaluation of the local kinematic and load distribution response of the model to any head impact or base impulsive loading. Mirsa and Chakravarty (1985) adopted a mathematical model of the human head consisting of an elastic prolate spheroidal shell (representing the skull) filled with a viscoelastic (Kelvin) material representing the brain tissue; the shell was supposed to be connected to a linear viscoelastic cantilever beam (representing the neck). Based on the above mentioned model they studied the dynamic response of a head-neck system to an impulsive load. Deng and Goldsmith (1987) developed a three-dimensional lumped - parameter model of a human head/neck/upper torso to predict its motion for any specified initial conditions.

The experimental investigations of the resonance frequencies of the human skull have been made on living subjects as well as cadavers and dry skulls. Khalil et al. (1979) presented a comprehensive investigation of the resonance frequencies of the human dry skull. The resonance frequencies of the human skull *in vivo* have been recently investigated by Håkansson et al. (1994).

In this study the cranial bone (skull) is approximated by a linear elastic homogeneous sphere and the brain material by an inviscid irrotational fluid. The neck support is approximated by an elastic support which reacts in three-dimensions. The main purpose of the present work is to investigate the eigenfrequencies of the head-neck system: the analysis is based on the three-dimensional theory of elasticity and the representation of the displacement field of the skull in terms of Navier eigenvectors (Hansen, 1935). The motion of the fluid is supposed to undergo small oscillations governed by the wave equation. The frequency equation is constructed by imposing the satisfaction of the boundary conditions and it is solved numerically. The results obtained are compared with the existing experimental ones. From the present analysis we lead to the conclusions that the neck support plays an important role on the eigenfrequencies of the human head, the neck model considered has to be improved by taking into account its viscoelastic behaviour and the skull -brain model has to be modelled as skull-fluid model with viscoelastic properties.

2. PROBLEM FORMULATION

The geometry chosen for the examination of the dynamical characteristics of the human head-neck system is shown in Figure 1:

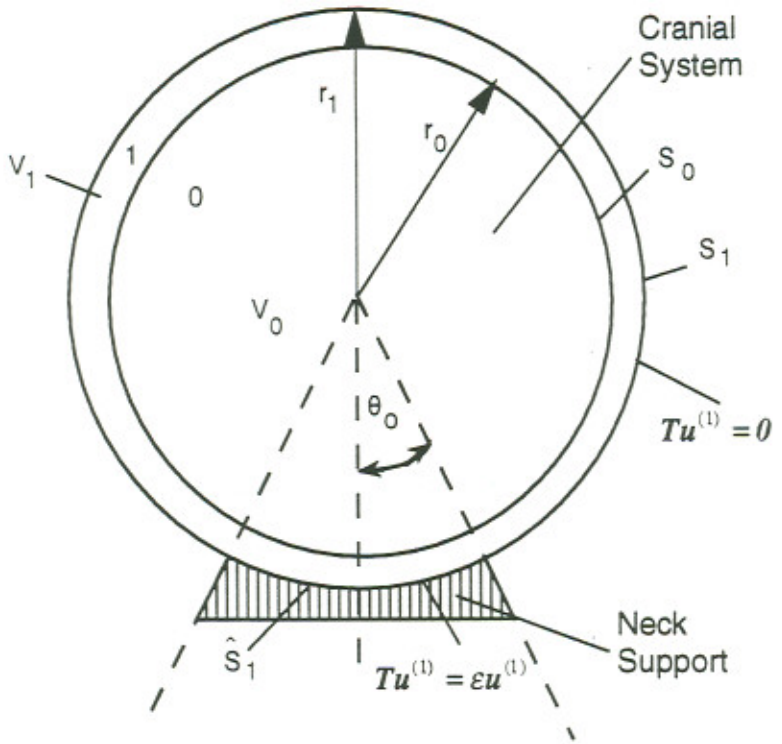

Figure 1: Human head-neck system

The cranial bone (skull) is approximated by a linear elastic homogeneous sphere (region 1) and the brain material by an inviscid, irrotational fluid (region 0). The neck support is identified as a region defined by the angle θ_0 and mathematically by different conditions than those on $S_1 \setminus \hat{S}_1$.

For the region 1 (elastic sphere) the displacement vector field $\boldsymbol{u} = \boldsymbol{u}(\boldsymbol{r},t)$ satisfies the equation:

$$\mu_1 \nabla^2 \boldsymbol{u}^{(1)}(\boldsymbol{r},t) + (\lambda_1 + \mu_1)\nabla\nabla\cdot\boldsymbol{u}^{(1)}(\boldsymbol{r},t) = \rho_1 \frac{\partial^2 \boldsymbol{u}^{(1)}(\boldsymbol{r},t)}{\partial t^2} \tag{1}$$

where μ_1 and λ_1 are Lamè's constants, ρ_1 is the mass density of the skull, ∇ is the del operator and t is the time.

For the free vibration problem we assume that

$$\boldsymbol{u}^{(1)}(\boldsymbol{r},t) = \boldsymbol{u}_o^{(1)}(\boldsymbol{r})e^{-i\omega t}, \tag{2}$$

where ω is the angular frequency measured in radians/sec and $i = \sqrt{-1}$.

Introducing the following dimensionless parameters

$$r' = \frac{r}{\alpha}, \quad \Omega = \frac{\omega\alpha}{c_{P_1}}, \quad (\alpha = r_1) \tag{3}$$

and replacing (2) into the equation of motion (1) we obtain

$$c'^{2}_{s1}\nabla'^{2}\boldsymbol{u}_o^{(1)}(\boldsymbol{r}')+(c'^{2}_{p1}-c'^{2}_{s1})\nabla'(\nabla'\cdot\boldsymbol{u}_o^{(1)}(\boldsymbol{r}'))+\Omega^2\boldsymbol{u}_o^{(1)}(\boldsymbol{r}')=0, \tag{4}$$

where

$$\nabla'=\alpha\nabla,\quad c'_{s1}=\frac{c_{s1}}{c_{P_1}},\quad c'_{s_1}=\frac{c_{P_1}}{c_{P_1}},\quad c^2_{s_1}=\frac{\mu_1}{\rho_1},\quad c^2_{P_1}=\frac{(\lambda_1+2\mu_1)}{\rho_1}.$$

The motion of an inviscid and irrotational fluid undergoing small oscillations is governed by the wave equation,

$$\nabla^2\Phi=\frac{1}{c_f^2}\frac{\partial^2\Phi}{\partial t^2}$$

or

$$\nabla'^{2}\Phi=\frac{1}{c'^{2}_{f}}\frac{\partial^2\Phi}{\partial t'^{2}}, \tag{5}$$

where Φ is the velocity potential, c_f is the speed of sound in the fluid and

$$t=\frac{\alpha}{c_{P_1}}t',\quad c'_f=\frac{c_f}{c_{P_1}}.$$

Supposing that

$$\Phi(\boldsymbol{r}',t')=\Phi_o(\boldsymbol{r}')e^{-i\Omega t'}$$

we obtain

$$\nabla'^{2}\Phi_o(r')=-k'^{2}_{f}\Phi_o(r') \tag{6}$$

where $k'_f=\Omega/c'_f$.

The pressure, P, in the fluid is found from the velocity potential as

$$P=-\rho_f\left(\frac{\partial\Phi}{\partial t}\right), \tag{7}$$

where ρ_f is the mass density of the fluid.

In nondimensionalised form the previous relation takes the form

$$P'=\frac{P}{\mu_1}=i\Omega\rho'_f\frac{1}{c'^{2}_{s}}\Phi_o(r')e^{-i\Omega t'}, \tag{8}$$

where $\rho'_f=\rho_f/\rho_1$.

The boundary condition satisfied by the elastic field on the exterior surface S_1 is of mixed type. More precisely, the surface section shown in Fig. 1 in the region $0\le\vartheta<\pi-\theta_o$ is stress free, while the surface section $\pi-\theta_0\le\vartheta\le\pi$ represents the neck support and the boundary condition satisfied there must incorporate the physical character of the interaction between human head and

neck. We assume that a Robin type boundary condition is satisfied, which simulates appropriately the dynamic character of the motion of the contact region.

The boundary condition on the surface S_1 is described by

$$\boldsymbol{T}\boldsymbol{u}_o^{(1)} = \begin{cases} \boldsymbol{0}, & 0 \le \vartheta < \pi - \theta_o \\ \varepsilon \boldsymbol{u}_o^{(1)}, & \pi - \theta_o \le \vartheta \le \pi \end{cases} \tag{9}$$

where ε is a constant depending on the physical characteristics of the human neck.

The dimensionless surface traction operator $\boldsymbol{T}'$ is given as follows

$$\boldsymbol{T}' = 2\mu'_1 r_1 \hat{\boldsymbol{r}} \cdot \nabla' + \lambda'_1 r_1 \hat{\boldsymbol{r}} \nabla' \cdot + \mu'_1 r_1 \hat{\boldsymbol{r}} \times \nabla', \tag{10}$$

where $\hat{\boldsymbol{r}}$ is the unit outward normal vector on the outer surface

The boundary conditions on S_o are given as

$$\boldsymbol{T}' \boldsymbol{u}_o^{(1)}(\boldsymbol{r}'_0) = -P'(\boldsymbol{r}'_0)\hat{\boldsymbol{r}} \tag{11a}$$

$$\hat{\boldsymbol{r}} \cdot \boldsymbol{u}_o^{(1)}(\boldsymbol{r}'_0) = \hat{\boldsymbol{r}} \cdot \boldsymbol{u}_o^{(0)}(\boldsymbol{r}'_0). \tag{11b}$$

From the physical point of view the condition (11a) says that the radial stress in the regions 1 and 0 at $r = r_o$ is equal and opposite to the fluid pressure, while (11b) represents the continuity condition on S_o.

In what follows we will discuss the systems:
(a) skull - neck system (SN - model).
(b) skull - brain - neck system (BSN - model)

In the second system the only boundary condition that has to be satisfied on the surface S_o is:

$$\boldsymbol{T}' \boldsymbol{u}_o^{(1)}(\boldsymbol{r}'_0) = \boldsymbol{0}. \tag{12}$$

We note that the problem described by the equations of motion (4) and (5) and the boundary conditions (9), (11) (or (12)) is a well-posed mathematical problem.

3. PROBLEM SOLUTION

Adopting the methodology followed by Charalambopoulos et al. (1996a), we expand the displacement fields in the regions 0 and 1 in terms of the Navier eigenfunctions (Hansen, 1935), which constitute a complete set of vector functions in the space of square integrable functions in the region occupied by the system under investigation. More precisely, the displacement field in the elastic skull (region 1) has the full expansion

$$\boldsymbol{u}_o^{(1)}(\boldsymbol{r}) = \sum_{n=0}^{\infty} \sum_{m=-n}^{n} \sum_{l=1}^{2} \left\{ \alpha_n^{m,l} \boldsymbol{L}_n^{m,l}(\boldsymbol{r}) + \beta_n^{m,l} \boldsymbol{M}_n^{m,l}(\boldsymbol{r}) + \gamma_n^{m,l} \boldsymbol{N}_n^{m,l}(\boldsymbol{r}) \right\}, \quad \boldsymbol{r} \in V_1 \tag{13}$$

where

$$\boldsymbol{L}_n^{m,l}(r') = \dot{g}_n^l(\Omega r') P_n^m(\hat{\boldsymbol{r}}) + \sqrt{n(n+1)} \frac{g_n^l(\Omega r')}{\Omega r'} \boldsymbol{B}_n^m(\hat{\boldsymbol{r}})$$

$$\boldsymbol{M}_n^{m,l}(r') = \sqrt{n(n+1)} g_n^l(k'_s r') \boldsymbol{C}_n^m(\hat{\boldsymbol{r}}) \tag{14}$$

$$N_n^{m,l}(r') = n(n+1)\frac{g_n^l(k'_s r')}{k'_s r'} P_n^m(\hat{r}) + \sqrt{n(n+1)}\left\{\dot{g}_n^l(k'_s r') + \frac{g_n^l(k'_s r')}{k'_s r'}\right\} B_n^m(\hat{r})$$

$$k'_{p_1} = \frac{\Omega}{c'_{p_1}} = \Omega, \quad k'_{s_1} = \frac{\Omega}{c'_{s_1}}, \quad \dot{g}_n^l(z) = \frac{d}{dz}(g_n^l) \tag{15}$$

and $g_n^1(z)$ and $g_n^2(z)$ represent the spherical Bessel functions of the first, $j_n(z)$, and second, $y_n(z)$, kind, respectively. The functions $P_n^m(\boldsymbol{r}')$, $B_n^m(\boldsymbol{r}')$ and $C_n^m(\boldsymbol{r}')$ defined on the unit sphere, are the vector spherical harmonics introduced by Hansen (1935) and in spherical polar coordinates (r, ϑ, φ) are given as follows

$$\begin{aligned}
\boldsymbol{P}_n^m(\hat{r}) &= \hat{r} Y_n^m(\hat{r}) \\
\boldsymbol{B}_n^m(\hat{r}) &= \frac{1}{\sqrt{n(n+1)}}\left\{\hat{\vartheta}\frac{\partial}{\partial\vartheta} + \hat{\varphi}\frac{1}{\sin\vartheta}\frac{\partial}{\partial\varphi}\right\} Y_n^m(\hat{r}) \\
\boldsymbol{C}_n^m(\hat{r}) &= \frac{1}{\sqrt{n(n+1)}}\left\{\hat{\vartheta}\frac{1}{\sin\vartheta}\frac{\partial}{\partial\varphi} - \hat{\varphi}\frac{\partial}{\partial\vartheta}\right\} Y_n^m(\hat{r}),
\end{aligned} \tag{16}$$

where $\hat{\vartheta}$ and $\hat{\varphi}$ are the unit vectors in ϑ and φ - directions respectively, $Y_n^m(\hat{r}) = P_n^m(\cos\vartheta)e^{im\varphi}$ are the spherical harmonics and $P_n^m(\cos\vartheta)$ are the well known Legendre functions.

The spherical polar coordinates of the real part of the displacement field as well as the expressions $\boldsymbol{TL}_n^{m,l}(\hat{r}')$, $\boldsymbol{TM}_n^{m,l}(\hat{r}')$ and $\boldsymbol{TN}_n^{m,l}(\hat{r}')$ are given by Charalambopoulos et al. (1996b).

The fields in the fluid region (0) are generated by the scalar potential $\Phi(\boldsymbol{r}', t')$ only. This fact imposes the fields in region 0 to be expanded only in terms of the functions $\boldsymbol{L}_n^{m,l}(\boldsymbol{r}')$. In addition to that the necessity to keep the regularity close to the origin requires the parameter l to be equal to 1, that is

$$\Phi_o(r') = \sum_{n=0}^{\infty}\sum_{m=-n}^{n}\left\{c_{m,n} g_n^1(k'_f r')\right\} P_n^m(\cos\vartheta) e^{im\varphi} e^{-i\Omega t'}. \tag{17}$$

The velocity of the fluid is expressed as

$$\boldsymbol{v}'(\boldsymbol{r}', t') = \nabla' \Phi = \sum_{n=0}^{\infty}\sum_{m=-n}^{n} c_{nm} \boldsymbol{L}_n^{m,1}(\boldsymbol{r}') e^{-i\Omega t'} \tag{18}$$

and the corresponding displacement field is

$$\boldsymbol{u}_0(\boldsymbol{r}', t') = \frac{i}{\Omega}\boldsymbol{v}(\boldsymbol{r}') = \frac{i}{\Omega}\sum_{n=0}^{\infty}\sum_{m=-n}^{n} c_{nm} \boldsymbol{L}_n^{m,1}(\boldsymbol{r}') e^{-i\Omega t'}. \tag{19}$$

The expression for the pressure is found by replacing the expression (18) for the velocity potential Φ into (8), that is

$$P'(r',t) = i\Omega\rho'_f \frac{1}{c'^2_s}\Phi(r',t')$$

$$= i\Omega\rho'_f \frac{1}{c'^2_s}\sum_{n=0}^{\infty}\sum_{m=-n}^{n} c_{nm} g_n^1(k'_f r') P_n^m(\cos\vartheta) e^{im\varphi} e^{-i\Omega t'} \tag{20}$$

The Navier eigenvectors $\boldsymbol{L}_n^{m,1}(\boldsymbol{r}')$, $\boldsymbol{M}_n^{m,1}(\boldsymbol{r}')$ and $\boldsymbol{N}_n^{m,1}(\boldsymbol{r}')$ (Hansen, 1935) as well as the result on them of the stress operator $\boldsymbol{T}'$ are expressed in terms of the spherical harmonics $\boldsymbol{P}_n^m(\hat{\boldsymbol{r}})$, $\boldsymbol{B}_n^m(\hat{\boldsymbol{r}})$ and $\boldsymbol{C}_n^m(\hat{\boldsymbol{r}})$, which constitute an orthonormal set of vector functions on the unit sphere. Finally, the orthogonality and independence of the vector spherical harmonics are used for the satisfaction of the boundary conditions on S_0 by following the steps presented by Charalambopoulos et al., (1996b).

In the case under discussion we have:

At $r = r_0$:

$$\boldsymbol{T}'\boldsymbol{u}^{(1)}(r'_0,t') = -P'(r'_0,t')\hat{\boldsymbol{r}}$$

or

$$\sum_{l=1}^{2}\left[\alpha_{n'}^{m',l} A_{n'}^l(r'_0) + \gamma_{n'}^{m',l} D_{n'}^l(r'_0)\right] = -i\Omega\rho'_f \frac{1}{c'^2_s} c_{n'm'} g_{n'}^1(k'_f r'_0) \tag{21a}$$

$$\sum_{l=1}^{2}\left[\alpha_{n'}^{m',l} B_{n'}^l(r'_0) + \gamma_{n'}^{m',l} E_{n'}^l(r'_0)\right] = 0 \tag{21b}$$

$$\sum_{l=1}^{2}\left[\beta_{n'}^{m',l} C_{n'}^l(r'_0)\right] = 0, \tag{21c}$$

where $n' = 0,1,2,\ldots,\quad |m'| \le n'$.

The functions $A_{n'}^l, B_{n'}^l, C_{n'}^l, D_{n'}^l$ and $E_{n'}^l$ are given in Appendix C. The continuity of the radial displacements on S_0 gives

$$\hat{\boldsymbol{r}}\cdot\boldsymbol{u}^{(1)} = \hat{\boldsymbol{r}}\cdot\boldsymbol{u}^{(0)}$$

or

$$\sum_{l=1}^{2}\left[\alpha_{n'}^{m',l}\dot{g}_{n'}^l(\Omega r'_0) + \gamma_{n'}^{m',l}\frac{g_{n'}^l(k'_s r'_0)}{k'_s r'_0}\right] = \frac{i}{c'_f} c_{n'm'} g_{n'}^1(k'_f r_0'), \tag{22}$$

where $k'_s = \dfrac{\Omega}{c'_s}$.

The satisfaction of the boundary conditions on S_1 requires complicated manipulations of the initial form of equation (9).

The boundary condition (9) can be written as

$$\boldsymbol{T}\boldsymbol{u}^{(1)}(\boldsymbol{r}'_1) = f(\hat{\boldsymbol{r}})\boldsymbol{u}^{(1)}(\boldsymbol{r}'_1), \quad \hat{\boldsymbol{r}} \in S^2 \text{ (the unit sphere)} \tag{23}$$

where

$$f(\hat{\boldsymbol{r}}) = \begin{cases} \varepsilon, & \hat{\boldsymbol{r}} \in \hat{S}_1 \\ 0, & \hat{\boldsymbol{r}} \in S_1 \setminus \hat{S}_1 \end{cases}$$

with $\hat{S}_1$ being the portion of S_1 defined by $\pi - \vartheta_0 \le \vartheta \le \pi$.

The function $f(\hat{\boldsymbol{r}})$ can be expanded in terms of the complete set of spherical harmonics $Y_n^m(\hat{\boldsymbol{r}}) = P_n^m(\cos\vartheta)e^{im\varphi}$ as follows,

$$f(\hat{\boldsymbol{r}}) = \sum_{n=0}^{\infty}\sum_{m=-n}^{n} k_{nm} Y_n^m(\hat{\boldsymbol{r}}). \tag{24}$$

It can be proved that the coefficients k_{nm} are given by the relation

$$k_{nm} = \begin{cases} 0 & m \neq 0 \\ \varepsilon\dfrac{\sqrt{\pi}}{2^n}\sqrt{2n+1}\displaystyle\sum_{k=0}^{\left[\frac{n}{2}\right]}\frac{(-1)^{n-k+1}(2n-2k)!}{k!(n-k)!(n-2k+1)!}\left[\cos\vartheta_0^{n-2k+1}-1\right], & m=0 \end{cases} \tag{25}$$

Consequently, the boundary condition (23) takes the form

$$\sum_{n=0}^{\infty}\sum_{m=-n}^{n}\sum_{l=1}^{2}\left\{\begin{array}{l}\left[\alpha_n^{m,l}A_n^l(r'_1)+\gamma_n^{m,l}D_n^l(r'_1)\right]\boldsymbol{P}_n^m(\hat{\boldsymbol{r}}) \\ +\left[\alpha_n^{m,l}B_n^l(r'_1)+\gamma_n^{m,l}E_n^l(r'_1)\right]\boldsymbol{B}_n^m(\hat{\boldsymbol{r}})+\beta_n^{m,l}C_n^m(r'_1)\boldsymbol{C}_n^m(\hat{\boldsymbol{r}})\end{array}\right\} =$$

$$\sum_{n=0}^{\infty}\sum_{m=-n}^{n}\sum_{l=1}^{2}\left\{\begin{array}{l}\left[\alpha_n^{m,l}\hat{A}_n^l(r'_1)+\gamma_n^{m,l}\hat{D}_n^l(r'_1)\right]\boldsymbol{P}_n^m(\hat{\boldsymbol{r}}) \\ +\left[\alpha_n^{m,l}\hat{B}_n^l(r'_1)+\gamma_n^{m,l}\hat{E}_n^l(r'_1)\right]\boldsymbol{B}_n^m(\hat{\boldsymbol{r}})+\beta_n^{m,l}\hat{C}_n^m(r'_1)\boldsymbol{C}_n^m(\hat{\boldsymbol{r}})\end{array}\right\}$$
$$\cdot\varepsilon\sqrt{\pi}\sum_{i=0}^{\infty}\frac{\sqrt{2i+1}}{2^i}\sum_{k=0}^{\left[\frac{i}{2}\right]}\frac{(-1)^{i-k+1}(2i-2k)!}{k!(i-k)!(i-2k+1)!}(\cos\vartheta_0^{i-2k+1}-1)Y_i^0(\hat{r}) \tag{26}$$

We take the inner product of the equation (26) with the vector harmonic functions $\boldsymbol{P}_{n'}^{m'}$, $\boldsymbol{B}_{n'}^{m'}$, $\boldsymbol{C}_{n'}^{m'}$ and successively we integrate over the unit sphere. In the right hand side, there emerge the integrals $\int_{S^2} Y_n^m Y_{n'}^{m'} Y_i^0 dS$, $\int_{S^2}\boldsymbol{B}_n^m\cdot\boldsymbol{B}_{n'}^{m'}Y_i^0 dS$, $\int_{S^2}\boldsymbol{C}_n^m\cdot\boldsymbol{C}_{n'}^{m'}Y_i^0 dS$, $\int_{S^2}\boldsymbol{B}_n^m\cdot\boldsymbol{C}_{n'}^{m'}Y_i^0 dS$ whose calculation requires extended and elaborate use of the properties of spherical harmonics. Finally, we obtain the following relations,

$$\sum_{l=1}^{2}\left[\alpha_{n'}^{m',l}A_{n'}^l(r'_1)+\gamma_{n'}^{m',l}D_{n'}^l(r'_1)\right] =$$
$$\sum_{n=|m'|}^{\infty}\sum_{l=1}^{2}\left[\alpha_n^{m',l}\hat{A}_n^l(r'_1)+\gamma_n^{m',l}\hat{D}_n^l(r'_1)\right]\Xi(n',n,\vartheta_0,m') \tag{27a}$$

$$\sum_{l=1}^{2}\left[\alpha_{n'}^{m',l}B_{n'}^{l}(r'_1)+\gamma_{n'}^{m',l}E_{n'}^{l}(r'_1)\right]= \sum_{n=|m'|}^{\infty}\sum_{l=1}^{2}\left[\alpha_{n}^{m',l}\hat{B}_{n}^{l}(r'_1)+\gamma_{n}^{m',l}\hat{E}_{n}^{l}(r'_1)\right]\Xi_1(n',n,\vartheta_0,m') \tag{27b}$$

and

$$\sum_{l=1}^{2}\beta_{n'}^{m',l}C_{n'}^{l}(r'_1)=\sum_{n=|m'|}^{\infty}\sum_{l=1}^{2}\beta_{n}^{m',l}\hat{C}_{n}^{l}(r'_1)\Xi_1(n',n,\vartheta_0,m') \tag{27c}$$

respectively, where

$$\Xi(n',n,\vartheta_o,m')=\varepsilon\sqrt{\pi}\sum_{\substack{i=|n'-n|\\ i-n'+n=even}}^{n+n'}\frac{\sqrt{2i+1}}{2^i}\sum_{k=0}^{[i/2]}\frac{(-1)^{i-k+1}(2i-2k)!}{k!(i-k)!(i-2k+1)!}\cdot$$

$$[(\cos\vartheta_o)^{i-2k+1}-1](-1)^{n-i+m'}\sqrt{2n'+1}\begin{pmatrix}n & i & n'\\ m' & 0 & -m'\end{pmatrix}$$

$$\Xi_1(n',n,\vartheta_o,m')=\varepsilon\sqrt{\pi}\sum_{\substack{i=|n'-n|\\ i-n'+n=even}}^{n+n'}\frac{\sqrt{2i+1}}{2^i}\sum_{k=0}^{[i/2]}\frac{(-1)^{i-k+1}(2i-2k)!}{k!(i-k)!(i-2k+1)!}\cdot$$

$$[(\cos\vartheta_o)^{i-2k+1}-1]\frac{1}{2}\left(\sqrt{\frac{n(n+1)}{n'(n'+1)}}+\sqrt{\frac{n'(n'+1)}{n(n+1)}}-\frac{i(i+1)}{\sqrt{(n(n+1)n'(n'+1)}}\right)\cdot$$

$$(-1)^{n-i+m'}\sqrt{2n'+1}\begin{pmatrix}n & i & n'\\ m' & 0 & -m'\end{pmatrix}$$

and

$$\begin{pmatrix}n & i & n'\\ m' & 0 & -m'\end{pmatrix}=$$

$$\left[\frac{(n+i-n')!(n-i+n')!(-n+i+n')!}{(n+i+n'+1)!}\right]^{1/2}\left[(n+m')!(n-m')!(i!)^2(n'-m')!(n'+m')!\right]^{1/2}$$

$$\sum_{z\in L}\frac{(-1)^{z+n+i+m'}}{z!(n+i-n'-z)!(n-m'-z)!(i-z)!(n'-i+m'+z)!(n'-n+z)!}$$

with

$$L=\{z\in Z:\max[n-n',i-n'-m',0]\le z\le\min[n+i-n',n-m',i]\}.$$

The algebraic equations (21), (22) and (27) consist of a linear system of the following form:

$$\boldsymbol{Dx}=\boldsymbol{0} \tag{28}$$

where

$$\boldsymbol{D}=\begin{bmatrix} \boldsymbol{D}_{|m'|,|m'|} & \boldsymbol{D}_{|m'|,|m'|+1} & \boldsymbol{D}_{|m'|,|m'|+2} & \cdots \\ \boldsymbol{D}_{|m'|+1,|m'|} & \boldsymbol{D}_{|m'|+1,|m'|+1} & \boldsymbol{D}_{|m'|+1,|m'|+2} & \cdots \\ \boldsymbol{D}_{|m'|+2,|m'|+1} & \boldsymbol{D}_{|m'|+2,|m'|+2} & \boldsymbol{D}_{|m'|+2,|m'|+3} & \cdots \\ \cdots & \cdots & \cdots & \cdots \end{bmatrix} \tag{29}$$

is a $7(n'+1)$ matrix for the BSN - Model and $6(n'+1)$ for the SN - Model, where n' ensures convergence and

$$\boldsymbol{x}=\left[\alpha_{|m'|}^{m',1},\alpha_{|m'|}^{m',2},\ldots,\gamma_{|m'|}^{m',1},c_{|m'|,m'},\alpha_{|m'|+1}^{m',1},\alpha_{|m'|+1}^{m',2},\ldots,\gamma_{|m'|+1}^{m',1},c_{|m'|+1,m'},\ldots\right]^{T}. \tag{30}$$

Details about the matrix $\boldsymbol{D}$, for each case under discussion, are given in Appendices A and B.

In order for the system (28) to have a non-trivial solution, the following condition has to be satisfied

$$\det(\boldsymbol{D})=0. \tag{31}$$

This condition provides the characteristic (frequency) equation, the roots of which are the eigenfrequency coefficients Ω of the system under investigation. The mode shape corresponding to each Ω can be obtained by solving the system (28).

4. NUMERICAL RESULTS - DISCUSSION - CONCLUSIONS

The frequency equation (31) has been solved numerically by using a matrix determinant computation routine along with a bisection method. The dimension of the matrix $\boldsymbol{D}$ depends on the value of n', which ensures convergence of Ω_k, $k=1,2,\ldots,20$. The computation of $\Omega_k=\Omega_k(\varepsilon,\theta_0,n')$ has been done by using an iterative procedure and the results obtained are cited in Table 1. We observe that the value of n' for convergence is strongly dependent on the values of ε and θ_0, $n'_{conv.}=n'(\varepsilon,\theta_0)$. In the case under discussion, for fixed values of ε and θ_0, the computational procedure was repeated until $\left\|\Omega_k^{(n')}-\Omega_k^{(n'+1)}\right\|\approx \mathrm{O}(10^{-4})$, $k=1,2,\ldots,20$. It is noted that the accuracy of the bisection method used is of the order of $\mathrm{O}(10^{-8})$ and the computing time needed is an increasing function of n'.

The elements of $\boldsymbol{D}$ are functions of Ω (see Appendices A and B) and therefore they have to be computed for every different value of it. This fact requires the computation of Spherical Bessel functions of the first and second kind as well as their derivatives. In our computations we have used Seed's method (Press et al., 1992) for the computation of Bessel functions of fractional order and their derivatives by using the definitions of spherical Bessel functions for integer n'. We note that recursive relations, although they offer flexibility and fast computations, are not valid for high values of n' and values of the argument close to zero.

Table 1: BSN - Model: Convergence of Ω_k, $k = 1,2,...,20$

$E_1 = 6.5x10^9\ N/m^2$, $\nu_1 = 0.25$, $\rho_1 = 2.1326x10^3\ Kg/m^3$, $K = 2.1029753x10^9\ N/m^2$, $\rho_f = 1.0002x10^3\ Kg/m^3$, $r_1 = 0.0854m$, $r_0 = 0.0794m$, $\varepsilon = -0.12$, $\theta_0 = \pi/8$

No.	n'=0	n'=1	n'=2	n'=3	n'=4	n'=5	n'=6	n'=7	n'=8	n'=9	n'=10	n'=11	n'=12	n'=13	n'=14	n'=15
1		0.1609	0.1686	0.1663	0.1672	0.1668	0.1670	0.1669	0.1670	0.1669	0.1670	0.1669	0.1670	0.1669	0.1669	0.1669
2		0.3793	0.4033	0.3955	0.3987	0.3973	0.3979	0.3977	0.3977	0.3977	0.3978	0.3977	0.3978	0.3977	0.3977	0.3977
3			0.4191	0.4259	0.4234	0.4242	0.4240	0.4241	0.4240	0.4241	0.4240	0.4241	0.4241	0.4240	0.4240	0.4240
4				0.5176	0.5183	0.5175	0.5182	0.5177	0.5180	0.5178	0.5179	0.5179	0.5179	0.5178	0.5178	0.5178
5					0.6283	0.6306	0.6300	0.6302	0.6301	0.6301	0.6301	0.6301	0.6301	0.6300	0.6300	0.6300
6						0.7362	0.7388	0.7376	0.7382	0.7379	0.7381	0.7380	0.7380	0.7379	0.7380	0.7380
7							0.8655	0.8659	0.8656	0.8658	0.8657	0.8658	0.8657	0.8657	0.8656	0.8656
8								1.0473	1.0484	1.0480	1.0482	1.0481	1.0481	1.0480	1.0480	1.0480
9			1.1787	1.1787	1.1787	1.1788	1.1787	1.1788	1.1787	1.1787	1.1787	1.1787	1.1787	1.1787	1.1787	1.1787
10		1.2071	1.2087	1.2081	1.2084	1.2082	1.2083	1.2083	1.2083	1.2083	1.2083	1.2083	1.2083	1.2064	1.2064	1.2064
11									1.2534	1.2538	1.2536	1.2537	1.2536	1.2535	1.2535	1.2535
12										1.5022	1.5024	1.5023	1.5024	1.5021	1.5022	1.5022
13											1.7864	1.7867	1.7866	1.7864	1.7864	1.7864
14				1.9119	1.9127	1.9124	1.9125	1.9125	1.9125	1.9125	1.9125	1.9125	1.9125	1.9125	1.9125	1.9125
15												2.0980	2.0981	2.0978	2.0978	2.0978
16			2.2356	2.2356	2.2356	2.2356	2.2356	2.2356	2.2356	2.2356	2.2356	2.2356	2.2356	2.2356	2.2356	2.2356
17	2.3691	2.3691	2.3691	2.3691	2.3691	2.3691	2.3691	2.3691	2.3691	2.3691	2.3691	2.3691	2.3690	2.3347	2.3347	2.3347
18													2.4412	2.4410	2.4409	2.4409
19					2.5415	2.5417	2.5415	2.5416	2.5415	2.5416	2.5416	2.5416	2.5416	2.5416	2.5416	2.5416
20														2.8081	2.8082	2.8082
21						3.1677	3.1678	3.1678	3.1678	3.1678	3.1678	3.1678	3.1678	3.1678	3.1678	3.1678
22															3.1976	3.1977
23														3.2411	3.2411	3.2411
24		3.2919	3.2919	3.2639	3.2641	3.2640	3.2640	3.2640	3.2640	3.2640	3.2640	3.2640	3.2640	3.2615	3.2615	3.2615

The numerical computations for the systems under discussion have been performed by using the following material properties:

Dry skull (McElhaney, 1970)

$$E = 1.379x10^9\ N/m^2,\ \ \nu = 0.25,\ \ \rho = 2.1326x10^3\ Kg/m^3,$$

Skull (Khalil and Hubbard, 1977)

$$E = 6.5x10^9\ N/m^2,\ \ \nu = 0.25,\ \ \rho = 2.1326x10^3\ Kg/m^3,$$

Cerebrospinal fluid (Khalil and Hubbard, 1977)

$$K = 2.1029753x10^9\ N/m^2,\ \ \rho = 1.0002x10^3\ Kg/m^3,$$

where E, K and ν denote the Young's modulus, bulk modulus and Poisson´s ratio, respectively. and $\lambda = \dfrac{E\nu}{(1+\nu)(1-2\nu)}$ and $\mu = \dfrac{E}{2(1+\nu)}$ are the Lamè´s constants.

Neck:

In the present analysis the neck is simulated by a system of springs which reacts in an isotropic way in three dimensions.

Taking into account the analysis by Landkof et al. (1976), we assumed that the values of the parameter ε vary as follows

$\varepsilon \in [-0.3, 0.0]$ for the SN - Model

and

$\varepsilon \in [-0.15, 0.0]$ for the BSN - Model.

The geometry of the skull - brain system is defined by:

$$r_1 = 0.0854m,\ \ r_0 = 0.0794m.$$

The determination of the support area is given by the angle θ_0 as

$\theta_0 \in \left[\dfrac{\pi}{50}, \dfrac{\pi}{15}\right]$, for the SN - Model

and

$\theta_0 \in \left[\dfrac{\pi}{50}, \dfrac{\pi}{8}\right]$, for the BSN - Model.

Since the analysis by Charalambopoulos et al. (1996a) gave very satisfactory results for the frequency spectrum of the dry skull, we adopted the SN - Model, although not realistic, to be studied in order to have an estimation of the influence of the neck support on the dynamic characteristics of the skull - neck system.

The effect of the neck - support on the eigenfrequencies of the SN - Model is presented in Tables 2 and 3 and graphically is shown in Figure 2. We observe that the neck introduces a pattern of additional frequencies to the spectrum of eigenfrequencies of the skull and also that the eigenfrequencies $\omega_k,\ k > 2$ suffer a shift as shown by the arrow in Figure 2.

Table 2: SN - Model: Variation of Ω_k, $k = 1,2,...,20$ with $\varepsilon \in [-0.3, 0.0]$

$E_1 = 1.379x10^9\ N/m^2$, $\nu_1 = 0.25$, $\rho_1 = 2.1326x10^3\ Kg/m^3$,

$r_1 = 0.0854m, r_0 = 0.0794m, \theta_0 = \pi/15$

No.	$\varepsilon = 0.0$	$\varepsilon = -0.1$	$\varepsilon = -0.2$	$\varepsilon = -0.3$
1		0.1416	0.2020	0.2497
2		0.1909	0.2733	0.3391
3	0.7070	0.7180	0.7301	0.7439
4	0.8492	0.8462	0.8411	0.8332
5	0.9419	0.9538	0.9697	0.9974
6	1.0500	1.0478	1.0415	1.0223
7	1.1954	1.1902	1.1840	1.1765
8	1.1963	1.2030	1.2106	1.2190
9	1.3883	1.3900	1.3921	1.3950
10	1.5456	1.5506	1.5528	1.5518
11	1.6255	1.6295	1.6360	1.6456
12	1.8897	1.8919	1.8937	1.8954
13	1.8901	1.8980		
14	1.9044	1.9068		
15	2.2201	2.2215	2.2230	2.2245
16	2.5359	2.5344	2.5327	2.5307
17	2.5683	2.5707	2.5732	2.5762
18	2.6218	2.6212	2.6203	2.6190
19	2.9451	2.9460	2.9470	2.9479
20	3.1627	3.1664	3.1701	3.1740

Table 3: SN - Model: Variation of Ω_k, $k = 1,2,...,20$ with $\theta_0 \in [0.0, \frac{\pi}{15}]$

$E_1 = 1.379x10^9\ N/m^2$, $\nu_1 = 0.25$, $\rho_1 = 2.1326x10^3\ Kg/m^3$,

$r_1 = 0.0854m, r_0 = 0.0794m, \varepsilon = -0.3$

No.	$\theta_0 = 0$	$\theta_0 = \frac{\pi}{100}$	$\theta_0 = \frac{\pi}{60}$	$\theta_0 = \frac{\pi}{30}$	$\theta_0 = \frac{\pi}{15}$
1		0.0366	0.0610	0.1225	0.2497
2		0.0495	0.0826	0.1659	0.3391
3	0.7070	0.7077	0.7091	0.7157	0.7439
4	0.8492	0.8489	0.8484	0.8457	0.8332
5	0.9419	0.9428	0.9446	0.9532	0.9974
6	1.0500	1.0496	1.0488	1.0451	1.0233
7	1.1954	1.1950	1.1943	1.1909	1.1765
8	1.1963	1.1972	1.1987	1.2050	1.2190
9	1.3883	1.3879	1.3874	1.3858	1.3950
10	1.5456	1.5460	1.5466	1.5491	1.5518
11	1.6255	1.6262	1.6273	1.6322	1.6456
12	1.8897	1.8899	1.8902	1.8914	1.8954
13	1.8901	1.8907	1.8918	1.8969	
14	1.9044	1.9041	1.9037	1.9029	
15	2.2201	2.2206	2.2213	2.2237	2.2245
16	2.5359	2.5356	2.5353	2.5337	2.5307
17	2.5683	2.5682	2.5679	2.5681	2.5762
18	2.6218	2.6218	2.6217	2.6212	2.6190
	2.9451	2.9455	2.9460	2.9474	2.9479
	3.1627	3.1631	3.1638	3.1667	3.1740

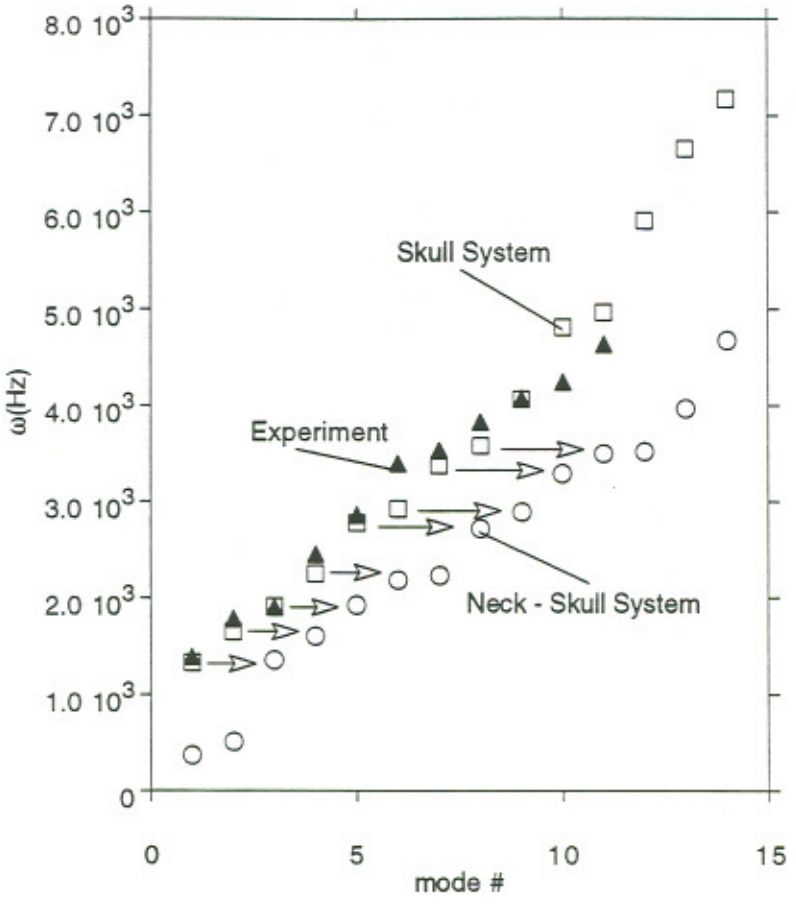

Figure 2: Comparison of ω_k for skull (Charalambopoulos et al., 1996) and skull - neck systems with experimental results for skull (Khalil et al., 1979).

$E_1 = 1.379x10^9\ N/m^2,\ \ \nu_1 = 0.25,\ \ \rho_1 = 2.1326x10^3\ Kg/m^3,$

$r_1 = 0.07735m, r_0 = 0.0691m, \varepsilon = -0.3, \theta_0 = \frac{\pi}{15}$

From the results cited in Tables 4 and 5, we observe that the influence of the neck - support on the eigenfrequencies of the BSN - Model is analogous to that on the SN - Model. The present model improves the results of the FF - Model (Charalambopoulos et al., 1996b). The first six eigenfrequencies predicted by the present analysis are very close to those measured experimentally, as it can be seen from the results presented in Table 6 and in Figure 3.

Table 4: BSN - Model: Variation of Ω_k, $k = 1,2,...,20$ with $\theta_0 \in [0.0, \frac{\pi}{8}]$

$E_1 = 6.5x10^9\ N/m^2$, $\nu_1 = 0.25$, $\rho_1 = 2.1326x10^3\ Kg/m^3$

$K = 2.1029753x10^9\ N/m^2, \rho_f = 1.0002x10^3\ Kg/m^3$

$r_1 = 0.0854m, r_0 = 0.0794m, \varepsilon = -0.12$

No.	$\theta_0 = 0$	$\theta_0 = \frac{\pi}{100}$	$\theta_0 = \frac{\pi}{50}$	$\theta_0 = \frac{\pi}{30}$	$\theta_0 = \frac{\pi}{15}$	$\theta_0 = \frac{\pi}{10}$	$\theta_0 = \frac{\pi}{8}$
1		0.0135	0.0271	0.0450	0.0897	0.1339	0.1669
2		0.0313	0.0626	0.1044	0.2096	0.3164	0.3977
3	0.3993	0.3995	0.4000	0.4013	0.4073	0.4163	0.4240
4	0.5172	0.5171	0.5169	0.5164	0.5149	0.5146	0.5178
5	0.6147	0.6149	0.6156	0.6173	0.6238	0.6293	0.6300
6	0.7239	0.7237	0.7234	0.7227	0.7223	0.7277	0.7380
7	0.8613	0.8615	0.8622	0.8636	0.8672	0.8669	0.8656
8	1.0350	1.0348	1.0345	1.0342	1.0360	1.0431	1.0480
9	1.1594	1.1578	1.1588	1.1611	1.1737	1.1747	1.1787
10		1.1953	1.1948	1.1937	1.1890	1.1901	1.2064
11	1.2459	1.2470	1.2475	1.2485	1.2496	1.2495	1.2535
12	1.4958	1.4956	1.4954	1.4953	1.4981	1.5017	1.5022
13	1.7790	1.7789	1.7793	1.7799	1.7803	1.7823	1.7864
14	1.8901	1.8904	1.8911	1.8928	1.8996	1.9077	1.9125
15	2.0934	2.0931	2.0930	2.0930	2.0956	2.0965	2.0978
16	2.2435	2.2409	2.2407	2.2402	2.2406	2.2361	2.2356
17	2.3641	2.3297	2.3298	2.3301	2.3655	2.3329	2.3347
18	2.4360	2.4357	2.4360	2.4363	2.4369	2.4393	2.4409
19	2.5359	2.5358	2.5355	2.5350	2.5341	2.5364	2.5416

Table 5: BSN - Model: Variation of Ω_k, $k = 1,2,...,20$ with $\varepsilon \in [-0.15, 0.0]$

$E_1 = 6.5x10^9\ N/m^2$, $\nu_1 = 0.25$, $\rho_1 = 2.1326x10^3\ Kg/m^3$

$K = 2.1029753x10^9\ N/m^2, \rho_f = 1.0002x10^3\ Kg/m^3$

$r_1 = 0.0854m, r_0 = 0.0794m, \theta_0 = \frac{\pi}{8}$

No.	$\varepsilon = 0.0$	$\varepsilon = -0.03$	$\varepsilon = -0.06$	$\varepsilon = -0.09$	$\varepsilon = -0.12$	$\varepsilon = -0.15$
1		0.0839	0.1184	0.1448	0.1669	0.1864
2		0.1918	0.2743	0.3400	0.3977	0.4317
3	0.3993	0.4048	0.4107	0.4171	0.4240	0.4510
4	0.5172	0.5183	0.5189	0.5189	0.5178	0.5157
5	0.6147	0.6180	0.6216	0.6257	0.6300	0.6350
6	0.7239	0.7273	0.7309	0.7345	0.7380	0.7414
7	0.8613	0.8627	0.8640	0.8650	0.8656	0.8660
8	1.0350	1.0379	1.0411	1.0446	1.0480	1.0518
9	1.1594	1.1695	1.1816	1.1846	1.1787	1.1715
10		1.1928	1.1892	1.1959	1.2064	1.2190
11	1.2459	1.2486	1.2504	1.2522	1.2535	1.2548
12	1.4958	1.4972	1.4989	1.5007	1.5022	1.5039
13	1.7790	1.7807	1.7826	1.7847	1.7864	1.7882
14	1.8901	1.8953	1.9008	1.9065	1.9125	1.9188
15	2.0934	2.0943	2.0955	2.0970	2.0978	2.0990
16	2.2435	2.2399	2.2386	2.2397	2.2356	2.2338
17	2.3641	2.3309	2.3322	2.3678	2.3347	2.3359
18	2.4360	2.4369	2.4382	2.4399	2.4409	2.4421
19	2.5359	2.5375	2.5389	2.5403	2.5416	2.5427

Table 6: Eigenfrequencies ω_k of the human head (Håkansson et al., 1994).

No.	Experimental Results (Håkansson et al., 1994) (mean values)	Standard Deviation (Håkansson et al., 1994)	FF - model (Charalambopoulos et al., 1996b)	Present Analysis (BSN - Model)
1	972	119	1423	595
2	1230	148	1843	1417
3	1532	159	2191	1511
4	1785	169	2580	1845
5	2076	217	3068	2245
6	2287	203	3636	2630
7	2568	308	4125	3085
8	2899	389	4261	3735
9	3253	381	4535	4201
10	3590	377	5775	4468
11	4101	543	6737	5354
12	4793	596	6920	6367
13	5304	660	7987	6816
14	5766	807	8303	7477
15	5841	419	8629	7968
16	6336	539	9040	8321
17	6656	429	11270	8700
18	6883	176	11560	9059
19	7165	.....	11580	10009

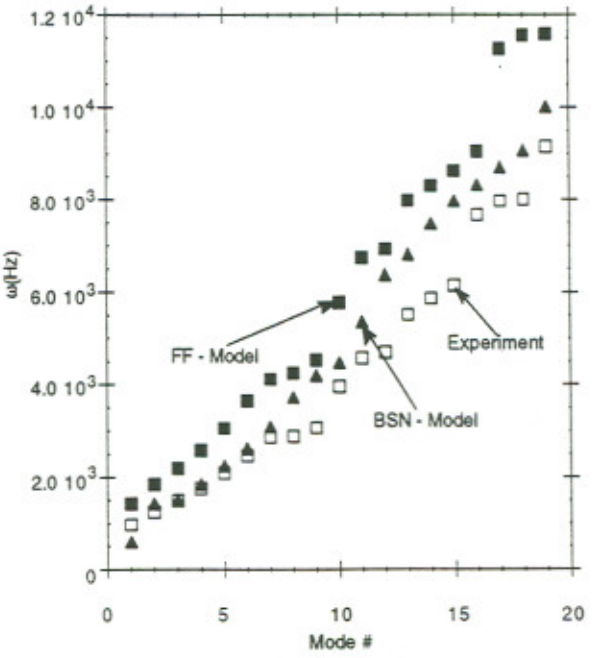

Figure 3: Comparison of ω_k for FF - Model and BSN - Model with experimental results (Håkansson et al. 1994).

$$E_1 = 6.5x10^9\ N/m^2,\ \ \nu_1 = 0.25,\ \ \rho_1 = 2.1326x10^3\ Kg/m^3$$
$$K = 2.1029753x10^9\ N/m^2, \rho_f = 1.0002x10^3\ Kg/m^3$$
$$r_1 = 0.0854m, r_0 = 0.0794m, \varepsilon = -0.12, \theta_0 = \frac{\pi}{8}$$

The variation of $\Omega_k,\ \ k = 1,2$ with the inner skull radius r_0 and the fluid density ρ_f are shown in Figures 4 and 5, respectively. We observe that the increase of ρ_f entails decrease of $\Omega_k,\ \ k = 1,2$, while increase of r_0 results increase of $\Omega_k,\ \ k = 1,2$.

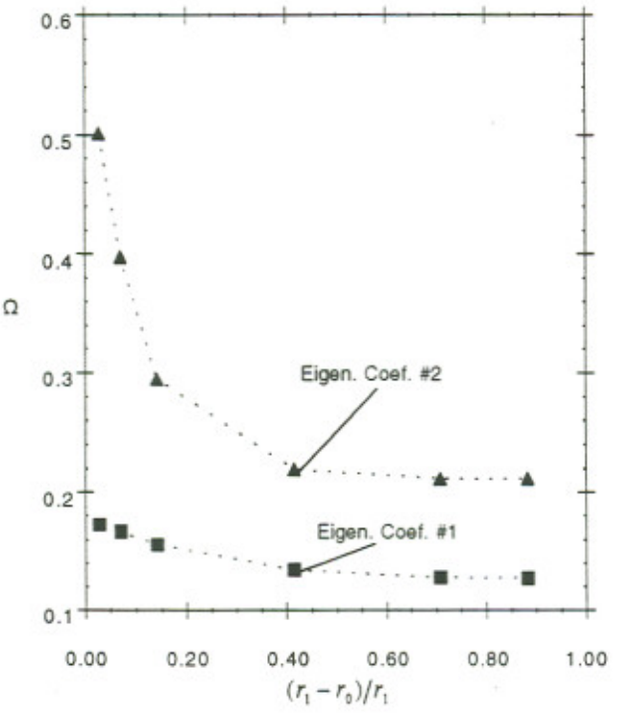

Figure 4: BSN - Model: Variation of $\Omega_k,\ \ k = 1,2$ with the inner skull radius r_0.

$$E_1 = 6.5x10^9\ N/m^2,\ \ \nu_1 = 0.25,\ \ \rho_1 = 2.1326x10^3\ Kg/m^3$$
$$K = 2.1029753x10^9\ N/m^2, \rho_f = 1.0002x10^3\ Kg/m^3$$
$$r_1 = 0.0854m, \varepsilon = -0.12, \theta_0 = \frac{\pi}{8}$$

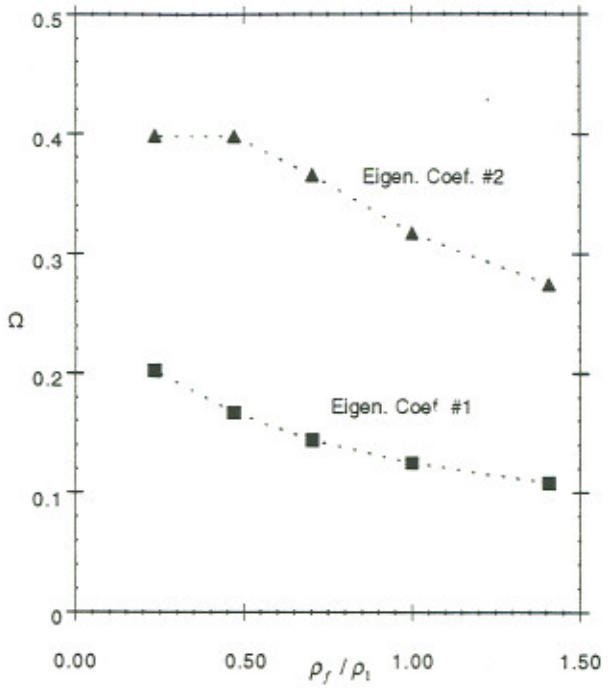

Figure 5: BSN - Model: Variation of Ω_k, $k = 1,2$ with the fluid density ρ_f.

$$E_1 = 6.5x10^9\ N/m^2,\ \ \nu_1 = 0.25,\ \ \rho_1 = 2.1326x10^3\ Kg/m^3$$

$$K = 2.1029753x10^9\ N/m^2$$

$$r_1 = 0.0854m, r_0 = 0.0794, \varepsilon = -0.12, \theta_0 = \frac{\pi}{8}$$

From the results presented we lead to the conclusions:

i. the neck support plays an important role on the dynamic characteristics of the human head
ii. the neck - model has to be improved by taking into account its viscoelastic behaviour
iii. the skull - brain system has to be modelled as skull - fluid model with viscoelastic properties

The improved model based on the above observations is under preparation and is scheduled to appear in a future communication.

ACKNOWLEDGEMENT

The present work forms part of the project "New Systems for Early Medical Diagnosis and Biotechnological Applications" which is supported by the Greek General Secretariat for Research and Technology through the EU funded R&D Program EPET II.

REFERENCES

Charalambopoulos A., Dassios G., Fotiadis D. I. , Kostopoulos V. , Massalas C. V., (1996), On the Dynamic Characteristics of the Human Skull, *International Journal of Engineering Science*, to appear.

Charalambopoulos A., Dassios G., Fotiadis D. I., Massalas C. V., (1996), "The Dynamic Characteristics of the Human Skull - Brain System", *Mathematical and Computer Modelling*, submitted.

Deng Y.C., and Goldsmith W., (1987) Response of a Human/Neck Upper - Torso Replica to Dynamic Loading - II. Analytical/Numerical Model, *J. Biomechanics*, **5**, 487-497.

Guarino J.R., (1982) Auscultatory percussion of the head, *British Medical Journal*, **284** 1075-1077.

Hansen W.W., (1935), A new type of expansion in radiation problems*Phys. Rev.* **47**, 139-143.

Hickling R. and Wenner M. L., (1973) Mathematical Model of a Head Subjected to an Axisymmetric Impact, *J. Biomechanics*, **6**, 115-132.

Huston R.L. and Sears J., (1981) Effect of Protective Helmet mass on Head/Neck Dynamics, *Transactions of the ASME*, **103**, 18-23.

Håkansson B. ,Brandt A. and Carlsson P., (1994) Resonance frequencies of the human skull *in vivo*, *J. Acoust. Soc. Am.* **95**(3), 1474 - 1481.

Kabo J.M., and Goldsmith W., (1983) Response of a Human Head-Neck Model to Transient Saggital Plane Loading, *J. Biomechanics*, **5**, 313-325.

Kenner V.H., and Goldsmith W., (1972) Dynamic Loading of a Fluid - Filled Spherical Shell, *Int. J. Mech. Sci.*, **14**, 557-568.

Khalil T.B. , Viano D.C. and Smith D.L. , Experimental Analysis of the Vibrational Characteristics of the Human Skull, *J. Sound and Vibration* **63**, 351, (1979).

Khalil T.B. and Hubbard R.P., (1977) Parametric Study Of Head Response by Finite Element Modelling, *J. Biomechanics*, **10**, 119-132.

Landkof B., Goldsmith W., and Sackman J.L., (1976) Impact on a Head-Neck Structure, *J. Biomechanics*, **9**, 141-151.

Lubock P. and Goldsmith W., (1980) Experimental Cavitation Studies in a Model Head - Neck System, *J. Biomechanics*, **13**, 1041-1052.

McElhaney J.H., Mechanical properties of Cranial Bone, (1970) *J. Biomechanics*, **3,** 495-511.

Merill T., Goldsmith W., and Deng Y.C., (1984) Three-Dimensional Response of a Lumped Parameter Head - Neck Model due to Impact and Impulsive Loading, *J. Biomechanics*, **17(2)** 81-95.

Misra J.C., and Chakravarty S., (1985) Dynamic Response of a Head-Neck System to an Impulsive Load, *J. Biomechanics*, **6**, 83-96.

Paddan G.S., and Griffin M.J., (1988) The Transmission of Translational Seat Vibration to the Head - I: Vertical Seat Vibration, *J. Biomechanics*, **21(3)**, 191-206.

Press W.H., Teukolsky S.A., Vetterling W.T. ,Flannery B.P., (1992) *Numerical Recipes in FORTRAN. The Art of Scientific Computing*, 2nd Edition, Cambridge University Press, Cambridge.

Reber J. G. and Goldsmith W., (1979) Analysis of Large Head - Neck Motions, *J. Biomechanics*, **12**, 211-222.

Williams J.L., (1988) Comment on the Paper 'Response of a Human Head/Neck/Upper-Torso Replica to Dynamic Loading - II. Analytical/Numerical Model, *J. Biomechanics*, **21(8)**, 687-692.

APPENDIX A: SN - Model

The matrix $\boldsymbol{D}$ can be described by a matrix of block elements having dimension 6 X 6, i.e.,

$$\boldsymbol{D} = \begin{bmatrix} \boldsymbol{D}_{1,1} & \boldsymbol{D}_{1,2} & \cdots & \boldsymbol{D}_{1,n'+1} \\ \boldsymbol{D}_{2,1} & \cdots & \cdots & \cdots \\ \cdots & \cdots & \cdots & \cdots \\ \boldsymbol{D}_{n'+1,1} & & & \boldsymbol{D}_{n'+1,n'+1} \end{bmatrix}$$

The diagonal elements $D_{k,k}$ are given as

$$\boldsymbol{D}_{k,k} = \begin{bmatrix} d_{1,1} & d_{1,2} & .. & .. & .. & d_{1,6} \\ d_{2,1} & .. & .. & .. & .. & .. \\ .. & & & & & \\ .. & & & & & \\ .. & & & & & \\ d_{6,1} & .. & .. & .. & .. & d_{6,6} \end{bmatrix}$$

where

$$d_{1,1} = A_k^1(r'_0),\ d_{1,2} = A_k^2(r'_0),\ d_{1,5} = D_k^1(r'_0),\ d_{1,6} = D_k^2(r'_0)$$

$$d_{2,1} = B_k^1(r'_0),\ d_{2,2} = B_k^2(r'_0),\ d_{2,5} = E_k^1(r'_0),\ d_{2,6} = E_k^2(r'_0)$$

$$d_{3,1} = A_k^1(r'_1) - \hat{A}_k^1(r'_1)\Xi(k,k,\vartheta_o,m'),\ d_{3,2} = A_k^2(r'_1) - \hat{A}_k^2(r'_1)\Xi(k,k,\vartheta_o,m'),$$

$$d_{3,5} = D_k^1(r'_1) - \hat{D}_k^1(r'_1)\Xi(k,k,\vartheta_o,m'),\ d_{3,6} = D_k^2(r'_1) - \hat{D}_k^2(r'_1)\Xi(k,k,\vartheta_o,m'),$$

$$d_{4,1} = D_k^1(r'_1) - \hat{D}_k^1(r'_1)\Xi(k,k,\vartheta_o,m'),\ d_{4,2} = D_k^2(r'_1) - \hat{D}_k^2(r'_1)\Xi(k,k,\vartheta_o,m'),$$

$$d_{4,5} = E_k^1(r'_1) - \hat{E}_k^1(r'_1)\Xi(k,k,\vartheta_o,m'),\ d_{4,6} = E_k^2(r'_1) - \hat{E}_k^2(r'_1)\Xi(k,k,\vartheta_o,m'),$$

$$d_{5,3} = C_k^1(r'_0),\ d_{5,4} = C_k^2(r'_0)$$

$$d_{6,3} = C_k^1(r'_1) - \hat{C}_k^1(r'_1)\Xi_1(k,k,\vartheta_o,m'),\ d_{6,4} = C_k^2(r'_1) - \hat{C}_k^2(r'_1)\Xi_1(k,k,\vartheta_o,m')$$

and the corresponding elements of the block submatrices $\boldsymbol{D}_{k,j}$ are

$$d_{3,1} = -\hat{A}_j^1(r_1)\Xi(k,j,\theta_0,m'),\ d_{3,2} = -\hat{A}_j^2(r_1)\Xi(k,j,\theta_0,m'),$$

$$d_{3,5} = -\hat{D}_j^1(r_1)\Xi(k,j,\theta_0,m'),\ d_{3,6} = -\hat{D}_j^2(r_1)\Xi(k,j,\theta_0,m'),$$

$$d_{4,1} = -\hat{B}_j^1(r_1)\Xi_1(k,j,\theta_0,m'),\ d_{4,2} = -\hat{B}_j^2(r_1)\Xi_1(k,j,\theta_0,m'),$$

$$d_{4,5} = -\hat{E}_j^1(r_1)\Xi_1(k,j,\theta_0,m'),\ d_{4,6} = -\hat{E}_j^2(r_1)\Xi_1(k,j,\theta_0,m'),$$

$$d_{6,3} = -\hat{C}_j^1(r_1)\Xi_1(k,j,\theta_0,m'),\ d_{6,4} = -\hat{C}_j^2(r_1)\Xi_1(k,j,\theta_0,m')$$

APPENDIX B: BSN - Model

The matrix $\boldsymbol{D}$ can be described by a matrix of block elements having dimension 7 X 7, i.e.,

$$\boldsymbol{D} = \begin{bmatrix} \boldsymbol{D}_{1,1} & \boldsymbol{D}_{1,2} & \cdots & \boldsymbol{D}_{1,n'+1} \\ \boldsymbol{D}_{2,1} & \cdots & \cdots & \cdots \\ \cdots & \cdots & \cdots & \cdots \\ \boldsymbol{D}_{n'+1,1} & & & \boldsymbol{D}_{n'+1,n'+1} \end{bmatrix}$$

The diagonal elements $D_{k,k}$ are given as

$$\boldsymbol{D}_{k,k} = \begin{bmatrix} d_{1,1} & d_{1,2} & \cdots & \cdots & \cdots & \cdots & d_{1,7} \\ d_{2,1} & \cdots & \cdots & \cdots & \cdots & \cdots & \cdots \\ \cdots & \cdots & \cdots & \cdots & \cdots & \cdots & \cdots \\ \cdots & \cdots & \cdots & \cdots & \cdots & \cdots & \cdots \\ \cdots & \cdots & \cdots & \cdots & \cdots & \cdots & \cdots \\ \cdots & \cdots & \cdots & \cdots & \cdots & \cdots & \cdots \\ d_{7,1} & \cdots & \cdots & \cdots & \cdots & \cdots & d_{7,7} \end{bmatrix}$$

where the only different elements from $\boldsymbol{D}_{k,k}$ corresponding to SN - Model are the following

$$d_{1,7} = -\frac{\Omega\rho'_f}{c'^2_s} g_k^1(k'_f r'_0),$$

$$d_{7,1} = \dot{g}_k^1(\Omega r'_0),\ d_{7,2} = \dot{g}_k^2(\Omega r'_0),\ d_{7,4} = k(k+1)\frac{g_k^1(k'_s r'_0)}{k'_s r'_0},\ d_{7,5} = k(k+1)\frac{g_k^2(k'_s r'_0)}{k'_s r'_0},$$

$$d_{7,7} = \frac{\dot{g}_k^1(k'_f r'_0)}{c'_f}$$

and the non-diagonal blocks have the same elements as in the case of the SN-Model (Appendix A) and the elements on the 7th row and column are zero.

APPENDIX C:

The functions $A^l_{n'}, B^l_{n'}, C^l_{n'}, D^l_{n'}, E^l_{n'}$ and $\hat{A}^l_{n'}, \hat{B}^l_{n'}, \hat{C}^l_{n'}, \hat{D}^l_{n'}, \hat{E}^l_{n'}$ are given as follows

$$A^l_{n,i}(r') = -\left[\frac{4\mu'_i}{r'}\dot{g}^l_n(k'_{pi}r') + 2\mu_i k'_{pi}\left(1-\frac{n(n+1)}{k'^2_{pi}r'^2}\right)g^l_n(k'_{pi}r') + \lambda'_i k'_{pi} g^l_n(k'_{pi}r')\right]$$

$$B^l_{n,i}(r') = 2\mu'_i\sqrt{n(n+1)}\left[\frac{1}{r'}\dot{g}^l_n(k'_{pi}r') - \frac{g^l_n(k'_{pi}r')}{k'_{pi}r'^2}\right]$$

$$\Gamma^l_{n,i}(r') = \mu'_i\sqrt{n(n+1)}\left[k'_{si}\dot{g}^l_n(k'_{si}r') - \frac{1}{r'}g^l_n(k'_{si}r')\right]$$

$$D^l_{n,i}(r') = 2\mu'_i n(n+1)\left[\frac{\dot{g}^l_n(k'_{si}r')}{r'} - \frac{g^l_n(k'_{si}r')}{k'_{si}r'^2}\right]$$

$$E^l_{n,i}(r') = \mu'_i\sqrt{n(n+1)}\left[-2\frac{\dot{g}^l_n(k'_{si}r')}{r'} - k'_{si}g^l_n(k'_{si}r') + 2\frac{n(n+1)-1}{k'_{si}r'^2}g^l_n(k'_{si}r')\right]$$

$$\hat{A}^l_{n'} = \dot{g}^l_{n'}(k'_p r')$$

$$\hat{B}^l_{n'} = \sqrt{n'(n'+1)}\frac{g^l_{n'}(k'_p r')}{k'_p r'}$$

$$\hat{C}^l_{n'} = \sqrt{n'(n'+1)}g^l_{n'}(k'_s r')$$

$$\hat{D}^l_{n'} = n'(n'+1)\frac{g^l_{n'}(k'_s r')}{k'_s r'}$$

$$\hat{E}^l_{n'} = \sqrt{n'(n'+1)}\left[\dot{g}^l_{n'}(k'_s r') + \frac{g^l_{n'}(k'_s r')}{k'_s r'}\right]$$